Developments in the Built Environment 26 (2026) 100892

Contents lists available at ScienceDirect

Developments in the Built Environment

journal homepage: www.sciencedirect.com/journal/developments-in-the-built-environment

Toward FAIR and reproducible research on air lime-containing mortars: characterization workflow and open dataset for fresh, physical, and mechanical properties

Guilherme da Silva Munhoz [*], Yu Zeng, Luiz Miranda de Lima Junior [1], Guang Ye

Civil Engineering, 3MD, Delft University of Technology, the Netherlands

ARTICLE INFO

Keywords:
FAIR principles
Reproducibility
Air lime
Mortar
Characterization

ABSTRACT

Although air lime is a carbonatable binder with high carbon sink potential, reproducible research remains hindered by the limited availability of lime-oriented standards and openly accessible datasets. These limitations prevent the consolidation of fundamental knowledge and reinforce the perception of lime mortars as highly variable and empirical materials. This study addresses this gap by implementing a FAIR-aligned (Findable, Accessible, Interoperable, Reusable) and reproducible workflow for the characterization of air lime-containing mortars. Four mixtures were monitored for up to 364 days to assess fresh, physical, and mechanical properties under defined conditions. All experimental metadata and datasets are openly published in a structured repository. Results show that air lime-containing mixtures exhibited longer setting times, higher open porosity, greater carbonation depths, and lower compressive strength. Length change measurements indicate hydration-carbonation interactions, particularly in lime-cement systems. By combining experimental characterization with a FAIR-aligned and reproducible workflow, this work supports more transparent, resource-efficient research practices.

1. Introduction

The lack of FAIR-aligned (Findable, Accessible, Interoperable, and Reusable) and reproducible workflows has increasingly been recognized as a critical challenge in modern research practices, limiting the consolidation of fundamental knowledge and the efficient use of resources (Wilkinson et al., 2016). Particularly in materials research, where experimental studies often characterize short- and long-term behavior of specimens under varying conditions, the lack of methodological detail during scientific reporting and the absence of openly accessible datasets hinder the comparability, verification, and reuse of results.

These challenges are particularly pronounced in the field of air lime mortars, a non-hydraulic, calcium-based binder historically associated with empirical practices and high variability (Kang et al., 2019). Air lime has been used as a building material since antiquity, with applications dating back to 7000 BCE (Carran et al., 2012; Arizzi and Cultrone, 2013; Lanas et al., 2004). Despite the improvements in lime production and construction techniques over the centuries, knowledge of lime-based materials remained poorly documented and was progressively lost following the widespread adoption of Portland cement (Hansen et al., 2008; Ruiz-Agudo and Rodriguez-Navarro, 2009).

Today, the use of building lime is mostly limited to the conservation of the built heritage and masonry systems (Oliveira et al., 2017). However, recent environmental policies, such as the European Green Deal (European Commission), have renewed interest in air lime mortars, as they harden primarily through carbonation, sequestering carbon dioxide (CO_2) and acting as carbon sinks (Liu et al., 2023). Over the past fifteen years, several studies investigating the physical and mechanical performance of lime-containing mortars were published, some of which are discussed in sequence.

At KU Leuven, extensive research has been conducted on lime-cement systems, particularly focusing on the interaction between cement hydration and lime carbonation (Van Balen, 2005; Cizer, 2009). At Trinity College Dublin, investigations have examined the influence of aggregate content on the physical and mechanical properties of

* Corresponding author.
E-mail addresses: g.dasilvamunhoz-1@tudelft.nl (G. da Silva Munhoz), y.zeng-4@tudelft.nl (Y. Zeng), luizc.limajunior@gmail.com (L.M. de Lima Junior), g.ye@tudelft.nl (G. Ye).
[1] Present address: Paebbl BV, The Netherlands.

https://doi.org/10.1016/j.dibe.2026.100892
Received 30 October 2025; Received in revised form 4 February 2026; Accepted 23 February 2026
Available online 28 February 2026

lime-containing mortars (Pavía and Aly, 2016; Pavia et al., 2019). Valuable insights into the characterization of lime-containing mortars have also been reported in Portugal (Oliveira et al., 2017; Branco et al., 2021), Spain (Lanas et al., 2005; Rodriguez-Navarro et al., 2023), Greece (Stefanidou et al., 2026; Pachta et al., 2014), and the United Kingdom (Lawrence et al., 2007; Ball et al., 2011).

From a standardization perspective, relevant frameworks include the EN 459 (European Committee for Standardization, 2015) and EN 1015 (European Committee for Standardization, 1998a) series, along with recent contributions from RILEM TC 277-LHS (Veiga et al., 2023; Groot et al., 2022; Alvarez et al., 2021; Maravelaki et al., 2023) and the European project SUBLime (SUBLime, 2021). The work of the RILEM TC 277-LHS committee in particular represents an important milestone in improving the testing and evaluation of lime-containing mortars. Four publications are worth mentioning.

i) *Properties of lime-based renders and plasters–discussion of current test methods and proposals for improvement* (Veiga et al., 2023) reviews the performance-related properties of lime-based renders and plasters. It highlights that many standardized test methods developed for cement-based mortars are not well suited to lime systems and proposes modifications to better characterize lime-based renders and plasters. These recommendations represent an initial step toward more reliable testing frameworks for lime-based materials.
ii) *Lime-based mortars for restoration–a review on long-term durability aspects and experience from practice* (Veiga et al., 2023) (Groot et al., 2022) synthesizes theoretical principles, laboratory research, and practical field experience to identify key limitations affecting the long-term durability of mortars used in the restoration of historic masonry. The report also stresses the need for careful evaluation and suitability testing to ensure compatible conservation interventions.
iii) *A review on the mechanisms of setting and hardening of lime-based binding systems* (Alvarez et al., 2021) consolidates existing knowledge on the physicochemical processes governing the setting and hardening of lime-based binders, including drying, carbonation, hydration, and pozzolanic reactions. The report emphasizes the need for adapted test methods that reflect the distinct composition and performance characteristics of lime-based systems.
iv) *Additives and admixtures for modern lime-based mortars* (Maravelaki et al., 2023) reviews the role of additives and admixtures in modern lime-based mortars, compiling knowledge from literature and practice. The report highlights the sensitivity of performance to dosage and the need for dedicated testing procedures and further standardization.

Despite the efforts reported in previous investigations (Oliveira et al., 2017; Van Balen, 2005; Cizer, 2009; Pavía and Aly, 2016; Pavia et al., 2019; Branco et al., 2021; Lanas et al., 2005; Rodriguez-Navarro et al., 2023; Stefanidou et al., 2026; Pachta et al., 2014; Lawrence et al., 2007; Ball et al., 2011), discussions on data transparency, FAIR alignment, and reproducibility remain scarce. Consequently, cross-study comparisons are limited, hindering the development of cumulative, interoperable datasets for lime mortar characterization. This gap directly affects the efficient use of research resources, as similar experimental efforts often need to be repeated rather than built upon.

Therefore, this work aims to support the transition toward more transparent and reproducible research practices in the field of air lime by combining experimental characterization with a FAIR-aligned workflow. Four mortar mixtures were designed and monitored for up to 364 days to assess fresh properties (entrapped air content and setting times), physical properties (pore structure, total length change, and mass evolution), and mechanical performance (compressive strength) under clearly defined material, curing, and environmental conditions. Carbonation progress was evaluated using the phenolphthalein indicator method and thermogravimetric analysis (TGA). All associated experimental metadata and datasets are openly published in a structured repository to support verification, reuse, and data integration. In the absence of dedicated lime-oriented standards, procedures established for Portland cement were adopted and fully documented to ensure reproducibility.

2. Materials and methods

Four mixtures were designed to investigate the fresh, physical, and mechanical properties of air lime-containing mortars. All mixtures followed a 1:3 binder-to-aggregate ratio, which has been widely reported in the literature (Cizer, 2009; Pavía and Aly, 2016) and is commonly employed in building practice. Although mixtures were named according to their volumetric proportions (as commonly specified in construction practice), all mixtures in this experimental program were proportioned by mass (as mass-based proportioning provides greater accuracy). The details of each mixture are presented in Table 1.

The water content in each mixture was adjusted to achieve a flow table value of 165 ± 8 mm, in accordance with EN 459-2:2021 (European Committee for Standardization, 2021). Maintaining a constant flow table value across mixtures is the standard approach in both research and field applications with air lime (Pavía and Aly, 2016; Pavia et al., 2019; Branco et al., 2021), as it ensures comparable workability and application techniques.

2.1. Materials

The mixtures were produced using Portland cement type II (CEM II/A-L 32.5R), hydrated air lime (CL90-S), standard siliceous sand (0-2 mm), and tap water. Portland cement type II was selected for its lower carbon footprint, resulting from the partial replacement of clinker with chemically inert limestone. Air lime type CL90-S was chosen for its high carbon sink potential, as its hardening mechanism depends primarily on carbonation. Standard siliceous sand (EN196-1:2016 (European Committee for Standardization, 2016)) was used to limit the number of variables within each mixture, given its controlled particle size distribution and chemical stability. A detailed characterization of each component is presented next.

2.1.1. Binders (Portland cement and air lime)

The chemical and mineral compositions of the binders were determined by X-ray fluorescence (XRF) and X-ray diffraction (XRD), respectively. The XRF results were obtained using a Panalytical Axios Max Wavelength Dispersive X-ray fluorescence spectrometer and are presented in Table 2. For the XRD analysis, scans were performed using a Bruker D8 Advance diffractometer coupled with Cu-Kα radiation ($\lambda = 1.54$ Å) over a 2θ range of 5°-75°, with a step size of 0.020°, and a counting time of 1.25 s per step. The XRD patterns are shown in Fig. 1.

According to Table 2, both binders exhibited high calcium contents. In Portland cement, this was attributed to the partial replacement of clinker with limestone filler, while in air lime, the high calcium content is intrinsic to its type (CL90-S). Regarding the mineral composition, XRD diffractograms revealed alite (C_3S), belite (C_2S), and calcium carbonate ($CaCO_3$) as the main crystalline phases in Portland cement. In air lime, calcium hydroxide ($Ca(OH)_2$) was identified as the predominant compound.

The physical characteristics of the binders, including bulk density, specific gravity, specific surface area (SSA), and median particle size (D_{50}) determined by laser diffraction, are presented in Table 3. Information on the particle size distribution was obtained using the Ankersmid EyeTech Laser diffraction analyzer and is shown in Fig. 2.

The SSA of the binders were measured by nitrogen (N_2) adsorption using the Brunauer-Emmett-Teller (BET) method. The higher values obtained for hydrated lime compared to cement are consistent with

Table 1
Mortar mixture proportions.

Code[a]	C:L:S[b] (volume)	w/b[c] (volume)	C:L:S[b] (mass)	w/b[c] (mass)	Cement (kg/m[c])	Lime (kg/m[c])	Sand (kg/m[c])	Water (kg/m[c])
C100L0	1:0:3	0.79	1:0:4.93	0.74	339.78	-	1676.66	251.84
C50L50	1:1:6	0.75	1:0.37:9.87	1.03	176.40	64.63	1740.96	248.26
C33L67	1:2:9	0.78	1:0.73:14.80	1.26	117.65	86.20	1741.64	256.34
C0L100	0:1:3	0.80	0:1:13.47	2.03	-	130.69	1760.30	265.30

[a] C100L0 represents a mixture with 100 % Portland cement and 0 % lime; C50L50 represents a mixture with 50 % Portland cement and 50 % lime; C33L67 represents a mixture with 33 % Portland cement and 67 % lime; and C0L100 represents a mixture with 0 % Portland cement and 100 % lime. The percentages are calculated based on the total binder volume.
[b] Cement:Lime:Sand.
[c] Water-to-binder ratio.

Table 2
Chemical composition of the binders determined using XRF.

Binder	CaO (%)	SiO_2 (%)	Al_2O_3 (%)	Fe_2O_3 (%)	SO_3 (%)	MgO (%)	K_2O (%)	TiO_2 (%)	Na_2O (%)	Others[a] (%)
Cement	73.16	15.44	3.67	3.13	2.54	0.92	0.37	0.28	0.19	0.30
Air lime	98.72	0.12	0.06	0.06	0.07	0.80	0.03	-	0.03	0.10

[a] It may include negligible contents of P_2O_5, SrO, Cl, ZnO, MnO, BaO, ZrO_2, PbO, Rb_2O, and Y_2O_3.

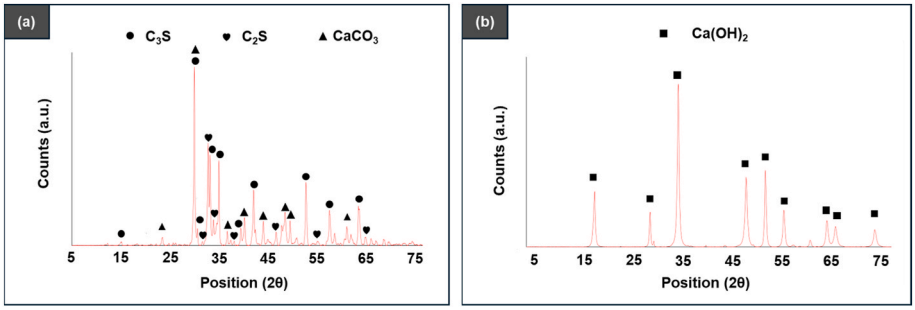

Fig. 1. Diffractograms from (a) cement and (b) lime powders.

Table 3
Physical characterization of the binders.

Properties	Cement (CEM II/A-L 32.5R)	Air lime (CL90-S)
Bulk density (kg/cm^3)	1068.47 ± 4.36	391.69 ± 3.67
Specific gravity (−)	3135.72 ± 10.70	2176.88 ± 71.59
Specific Surface Area (m^2/g)	1.30	13.50
D_{50} – Laser diffraction (μm)	26.23	10.54

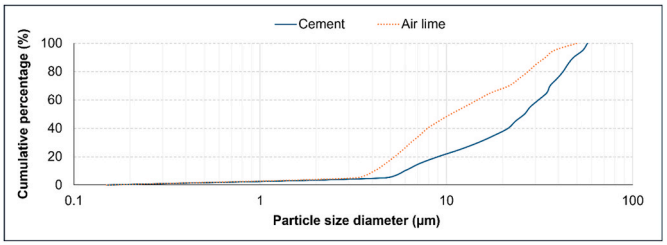

Fig. 2. Particle size distribution of cement and air lime using laser diffraction.

values reported in the literature (Fourmentin et al., 2015), where lime typically exhibits significantly greater surface area due to its finer and more porous particle structure.

As shown in Table 3 and Fig. 2, the D_{50} of Portland cement was about two times larger than that of air lime. Consequently, lime particles are expected to occupy the space between cement grains and play a physical role in addition to their chemical one.

2.1.2. Fine aggregate

The mineralogical composition of the fine aggregate was determined by XRD over a 2θ range of 5°-75°, with a step size of 0.020° and a counting time of 1.25 s per step. As shown in Fig. 3a, SiO_2 (quartz) was identified as the main crystalline phase. The particle size distribution of the sand was consistent with the recommendations of EN 196-1:2016 (European Committee for Standardization, 2016), as presented in Fig. 3b.

The physical characteristics of the fine aggregate, including bulk density, specific gravity, and water absorption are presented in Table 4.

The low water absorption seen in Table 4 indicates that the fine aggregate has low porosity and is, therefore, less prone to moisture retention. The measured bulk density and specific gravity are consistent with the expected values for siliceous sands.

2.2. Methods

2.2.1. Mixing, curing, and demolding

The mixing procedure lasted 4 min and followed the recommendations of EN 459-2:2021 (European Committee for Standardization, 2021) and EN 196-1:2016 (European Committee for Standardization, 2016). First, the binder was placed in the mixing bowl (for lime-cement systems, a manual pre-mix was performed). Then, water was added, and mixing proceeded at low speed for 30 s. During the following 30 s, sand was gradually added. After that, the mixing speed was set to high for another 30 s. For the subsequent 90 s, the mixer was switched off, and the sides and bottom of the bowl were scraped, including the shovel. Finally, mixing resumed at high speed for the remaining 60 s, stopping at 4 min. When necessary, tests on the fresh properties were conducted; otherwise, the mortars were cast into lubricated molds measuring

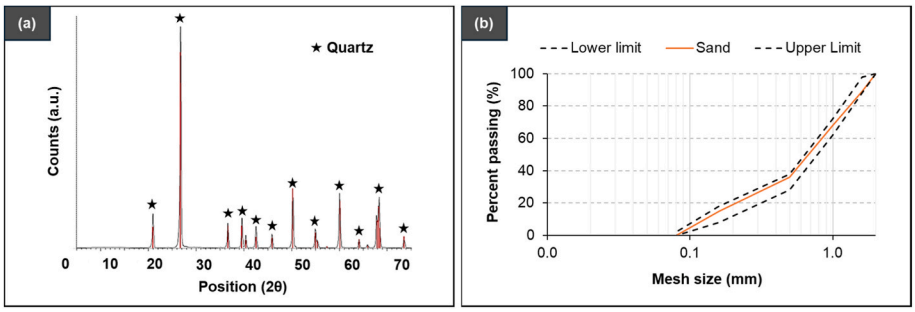

Fig. 3. Fine aggregate: (a) Diffractogram of the sand particles and (b) particle size distribution.

Table 4
Physical properties of the standard sand.

Material	Bulk density (kg/cm^3)	Specific gravity (−)	Water absorption (%)
Standard sand	(1763.55 ± 14.64)	(2622.98 ± 27.63)	(0.07 ± 0.01)

10 × 10 × 40 cm or 4 × 4 × 16 cm.

The curing conditions followed EN 1015-11:2019 (European Committee for Standardization, 2019a), with additional considerations. According to EN 1015-11:2019 (European Committee for Standardization, 2019a), mixtures containing cement (or air lime accounting for less than 50 % of the binder volume) must be demolded between one and three days after casting. Pure air lime mixtures, or those in which the air lime content exceeds 50 % of the binder volume, must be demolded after five days. Regardless of their composition, all specimens should be cured at 95 % RH and 21 °C until seven days after casting.

However, after several demolding attempts, it was observed that the pure lime specimens (C0L100) could not be demolded after five days without being damaged (see Fig. 4). This group depends primarily on carbonation for hardening, and at 95% RH the pores remain saturated, hindering the ingress of CO_2. Therefore, an adaptation to the curing procedure of C0L100 was required.

After a few preliminary tests combining different curing conditions to ensure a non-damaging demolding process, it was decided to cure the pure lime specimens for seven extra days, but at 55 % RH and 21 °C. Therefore, in addition to the initial seven days of curing under 95 % RH and 21 °C, following EN 1015-11:2019 (European Committee for Standardization, 2019a), the pure lime specimens were cured for seven more days and demolded after a total of 14 days. After the initial curing period, the specimens from all groups were kept and tested at (21 ± 2) °C and (55 ± 5) % RH; except for C100L0, which cured for 28 days at 95 % RH, in accordance with EN 12390-16:2019 (European Committee for Standardization, 2019b).

2.2.2. *Fresh properties*

In the fresh state, the four mixtures (C100L0, C50L50, C33L67, and C0L100) were tested for entrapped air content and setting time. The entrapped air content was determined following ASTM C185:2020 (American Society for Testing Materials, 2020) and EN 1015-6:1998 (European Committee for Standardization, 1998b); and the initial and final setting times were measured according to ASTM C403:2017 (American Society for Testing Materials, 2017) and ASTM C191:2021 (American Society for Testing Materials, 2021). An automatic Vicat apparatus was used to determine the setting times.

2.2.3. *Pore structure*

The pore structure was characterized through tests on open porosity, water absorption, and capillary suction, following the recommendations of ABNT NBR 9778:2005 (Associação Brasileira de Normas Técnicas, 2005) and EN 1015-18:2002 (European Committee for Standardization, 2003), respectively. Specimens measuring 4 × 4 × 16 cm were analyzed at 28, 91, 182, and 364 days after casting. The results represent the statistically treated average of three replicates per mixture per age.

Prior to the open porosity and water absorption tests, specimens

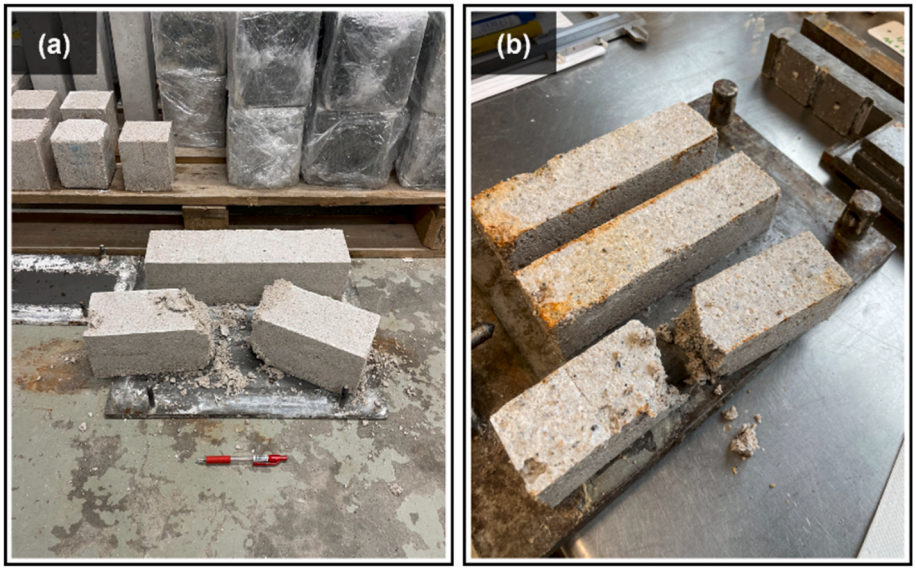

Fig. 4. Failed demolding attempts of specimens measuring (a) 10 × 10 × 40 cm; and (b) 4 × 4 × 16 cm.

were oven-dried at 60 °C for 48 h, until constant mass. The specimens were then immersed in water for 72 h, in accordance with ABNT NBR 9778:2005 (Associação Brasileira de Normas Técnicas, 2005). Open porosity was determined using the boiling-water saturation method (Associação Brasileira de Normas Técnicas, 2005), which promotes the removal of entrapped air and ensures complete filling of accessible pores.

For the capillary suction test, specimens were also oven-dried at 60 °C for 48 h until constant mass. They were then split in half, and the fractured surface was placed in contact with a 5-10 mm layer of water. The lateral sides and top surface were sealed to prevent evaporation and ensure unidirectional capillary uptake. The procedure for mortars other than renovation mortars described in EN 1015-18:2002 (European Committee for Standardization, 2003) was followed.

Additionally, the pore structure of the hardened mortar specimens was analyzed via mercury intrusion porosimetry (MIP) using the Micrometrics PoreSizer 9500 (instrument error ±2 %). Mortar samples were collected at 28, 91, 182, and 364 days after casting. Sample preparation and testing followed the recommendations of Berodier et al. (2016) and included: (i) extraction of cubic samples of approximately 1 cm^3 from depths between 5 and 15 mm to minimize edge effects; (ii) immersion of the samples in isopropanol for 28 days as part of the solvent-exchange procedure, followed by freeze-drying when MIP analysis could not be performed immediately; and (iii) placement of each sample in the penetrometer and degassing under vacuum to remove air from accessible porosity, after which the penetrometer was progressively filled with liquid mercury under vacuum for low- and high-pressure intrusion stages. A contact angle of 141° was used for data processing.

2.2.4. Total length change

The procedures for assessing length change were adapted from Portland cement-based standards, namely ASTM C1698:2019 (American Society for Testing Materials, 2019) (autogenous shrinkage) and EN 12390-16:2019 (European Committee for Standardization, 2019b) (total shrinkage). The autogenous shrinkage test was an additional experiment performed to capture early-age deformation, for up to 28 days after casting. Corrugated tubes containing fresh mixture were monitored using linear variable differential transformers (LVDTs). Total length change was determined using prismatic specimens (10 × 10 × 40 cm) with dial gauges (±0.001 mm) for up to 182 days. The results represent the statistically treated average of four replicates for autogenous shrinkage and two replicates for total length change, accounting for four datapoints. All tests were conducted in a controlled environment, at (55 ± 5) % RH and (21 ± 2) °C.

2.2.5. Compressive strength

The compressive strength of the four mortar mixtures was evaluated according to EN 1015-11:2019 (European Committee for Standardization, 2019a) and EN 12390-3:2019 (European Committee for Standardization, 2019c). Cubic specimens measuring 10 × 10 × 10 cm were tested at 28, 91, 182, and 364 days using a universal testing machine. The loading rate was set to 50 N/s for pure lime, 400 N/s for lime-cement, and 2400 N/s for pure cement specimens. The reported results represent the statistically treated average of three replicates.

2.2.6. Additional experiments

Additional characterization tests were performed to complement the physical and mechanical investigations. The progress of carbonation was assessed using phenolphthalein and TGA.

- **Mass monitoring:** The mass of the four mortar groups was monitored for 182 days as an indirect assessment of carbonation, since the conversion of $Ca(OH)_2$ to $CaCO_3$ results in an increase in mass and volume (Roy et al., 1999; Dheilly et al., 2002). Two specimens (10 × 10 × 40 cm) per group were monitored by using a digital scale (±0.1 g; 10 kg capacity).
- **Carbonation depth:** After the total length change test, at 182 days, the 10 × 10 × 40 cm specimens were split in half, and a phenolphthalein indicator was sprayed on their fractured surface. The recommendations from the RILEM TC 281-CCC (von Greve-Dierfeld et al., 2020) were followed and Carbonation depth was measured with a precision ruler (±0.25 mm).
- **TGA:** Samples were collected from the cross-section of the 4 × 4 × 16 cm specimens, at depths between 5 mm and 15 mm, and crushed to powder. Approximately 40 mg of powder was analyzed in a thermal analyzer NETZSCH TG-499-F3-Jupiter, heated from ambient temperature to 1000 °C, at a rate of 10 K/min. An argon atmosphere was used to prevent additional carbonation during the test. The recommendations from Lothenbach et al. (2016) were followed and samples were analyzed at 28, 91, 182, and 364 days after casting.

2.2.7. FAIR data and reproducibility considerations

In addition to experimental characterization, this study was designed to align with the FAIR (Findable, Accessible, Interoperable, and Reusable) principles and to support a reproducible workflow. Therefore, all datasets generated in this work are deposited in an open-access repository with a persistent identifier (DOI), structured metadata, and standardized file formats to ensure findability and accessibility. Prior to publication in the repository, the datasets were reviewed for completeness, metadata quality, and file integrity.

Interoperability was achieved through the use of SI units, standardized terminology, and widely readable file formats (i.e., .csv, .xls). Reusability and reproducibility were addressed by providing detailed documentation of materials, specimen preparation, curing conditions, test procedures, and equipment models. These measures enable independent verification, knowledge-building, and a more efficient use of research resources by reducing unnecessary duplication of experimental efforts.

3. Results and discussion

3.1. Fresh properties

The results on entrapped air content presented in Table 5 suggest that mixtures richer in air lime exhibit lower entrapped air. This behavior aligns with the median particle size (D_{50}) of the binders. Since air lime particles are smaller than cement particles (Table 3), they initially act as fillers, reducing the amount of entrapped voids in the fresh state.

Although the test performed according to ASTM C185:2020 (American Society for Testing Materials, 2020) and EN1015-6:1998 (European Committee for Standardization, 1998b) is not sufficient to discriminate the size of the entrapped bubbles, it is well established in the literature that entrapped air voids can reach the millimeter scale (Mehta and Monteiro, 2006), thereby affecting strength and pore network connectivity. The influence of entrapped air on the pore structure of hardened mortars is further discussed in *3.2 Pore structure*.

The results for bulk density are also presented in Table 5. As

Table 5
Properties of the fresh mixtures.

Codes	Entrapped air (%)	Theoretical bulk density (g/cm^3)	Real bulk density (g/cm^3)	Initial setting (HH:MM:SS)	Final setting (HH:MM:SS)
C100L0	7.10	2.27	2.11	01:48:00	04:38:00
C50L50	6.90	2.23	2.08	03:28:00	08:37:43
C33L67	5.80	2.20	2.07	04:32:00	12:30:00
C0L100	5.33	2.16	2.04	33:22:50	35:22:50

observed, mixtures with higher cement content exhibited greater densities. While higher air contents would typically reduce density, the results indicate that the higher density of the solid particles prevailed over the influence of air voids. For instance, the bulk density of Portland cement is nearly three times higher than that of air lime (Table 3). Furthermore, when theoretical and measured values were compared, the latter were consistently lower. This difference can be explained by particle packing and the presence of interstitial air, as suggested by Santos et al. (2018).

The setting times, presented in Table 5, indicate that as the lime content increased, both the initial and final setting times were delayed. Faster setting was observed in mixtures with higher Portland cement content. According to Cizer (2009), under normal environmental conditions, the hydration of clinker occurs more rapidly than the carbonation of air lime. In this study, the pure lime mixture required approximately three times longer to reach the final setting compared with the pure cement mixture. It should be noted, however, that the tests were conducted at 55 % RH, which may have facilitated excess water evaporation and, consequently, accelerated the setting process.

Hence, at early ages, the setting of air lime-rich mixtures depends primarily on the evaporation of excess water, which promotes pore desaturation and enables the ingress of CO_2. Nevertheless, under normal environmental conditions, the availability of CO_2 is limited (approximately 0.04 %, or 400 ppm), which also slows the overall hardening process, as reported by Arizzi and Cultrone (Arizzi et al., 2013) and Cizer (2009).

3.2. Pore structure

The pore structure was indirectly assessed through measurements of open porosity, water absorption, and capillary suction. The results for open porosity and water absorption are presented in Fig. 5a and b, respectively.

The open porosity results presented in Fig. 5a are consistent with the water absorption data shown in Fig. 5b. This behavior is expected, as both parameters are related to surface-accessible pores. A similar trend was reported by Medeiros-Junior et al. (de Medeiros-Junior et al., 2019), who suggested that open porosity is directly proportional to the material's capacity for water absorption.

In contrast to the behavior observed in the fresh state, where cement-rich mixtures exhibited the highest entrapped air content, the opposite trend was observed in the hardened state. According to the open porosity (Fig. 5a) and water absorption (Fig. 5b) results, cement-rich mixtures yielded the lowest porosity values. This behavior suggests that cement hydration contributed to a denser and more consolidated microstructure, reducing the overall porosity. Conversely, in lime-containing mixtures, the slow rate of carbonation sems to have delayed microstructural consolidation, which explains their higher open porosity and water absorption values compared with the cement-rich ones.

The highest open porosity and water absorption values were, however, observed in the lime-cement systems, where the competition for moisture between hydration and carbonation dictates a distinctive behavior. As explained by Cizer (2009), in such systems, the available moisture is used for cement hydration, CO_2 dissolution, and is partly evaporated. At low RH environments, this competition reduces the efficiency of both hydration and carbonation, leading to an incomplete formation of solid phases and a more porous microstructure, which explains the results shown in Fig. 5.

For C0L100, the high water retention capacity of air lime helps maintain internal moisture, promoting gradual carbonation and limiting moisture loss. In this case, much of the retained water is entrapped within the lime matrix and is slowly released over time, reducing the formation of large voids during drying (Pavía and Aly, 2016; Veiga, 2017). Consequently, although the total porosity and water absorption values may remain high, they tend to be lower compared with lime-cement mortars, as seen in Fig. 5.

Additionally, the open porosity results presented in Fig. 5a were compared with those obtained through MIP, as shown in Fig. 6a.

Figs. 5a and 6a yielded porosity values of similar magnitude. However, the MIP porosity was consistently higher, particularly for air lime-rich mixtures. A similar trend was reported by Arandigoyen et al. (2005), who attributed the higher porosity values obtained by MIP to the pressurized nature of the technique. Depending on mixture composition and curing age, air lime-containing specimens may lack sufficient mechanical strength to withstand the intrusion pressure, leading to microcracking and a potential overestimation of porosity, as noted by Cizer (2009). Nevertheless, the overall trends observed in Fig. 6a were consistent with those from Fig. 5a, supporting the interpretations discussed in the previous section. These observations are also in agreement with the findings of Arandigoyen and Alvarez (2007), who reported limited variation in total porosity across mixtures with different binder-to-aggregate ratios and cement-lime proportions. In their study, porosity remained almost invariable (ranging from 20 to 23%), suggesting that changes in binder and aggregate ratios do not necessarily lead to proportional variations in total porosity.

The results of the capillary suction tests are presented in Fig. 6b. Although capillary suction is primarily governed by pores formed during drying, typically ranging from 0.01 μm to 1 μm (Mehta and Monteiro, 2006), Pavía and Treacy (2006) noted that it is also influenced by the tortuosity and interconnectivity of the pore network. In air lime-cement systems, the interaction between binders with distinct particle size distributions combined with the competition for moisture during hydration and carbonation likely disrupted the pore network, which helps explain the irregular behavior observed for these mixtures. Hence, a direct relationship between lime content and capillary suction could not be established.

In contrast, the pure cement and pure lime groups generally exhibited an increase in capillary suction over time attributed to the precipitation of solid phases and the progressive consolidation of the microstructure. This reduction observed at 364 days may be associated with the excessive precipitation of $CaCO_3$ at later ages, as reported by Munhoz and Ye (da Silva Munhoz and Ye, 2025), which can induce microcracking, alter the pore structure, and consequently limit capillary

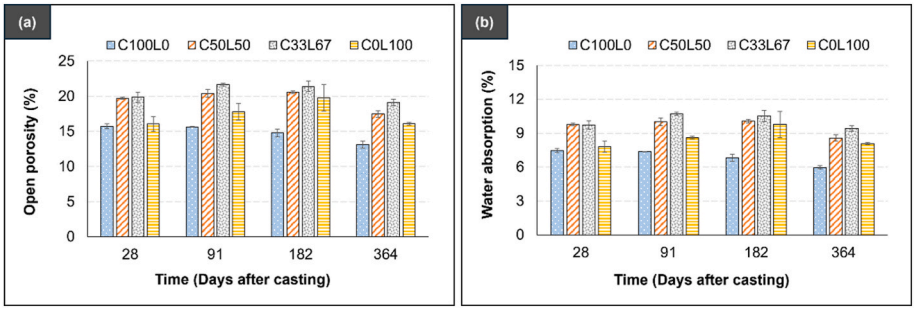

Fig. 5. Results on the (a) open porosity and (b) water absorption.

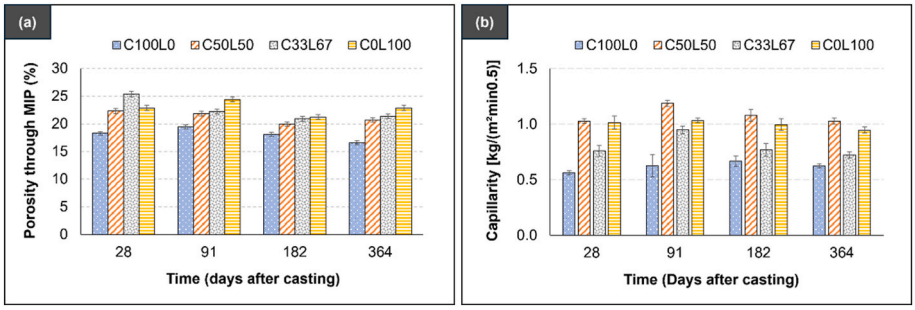

Fig. 6. Results on the (a) porosity measured through MIP and (b) capillary suction.

suction. Nevertheless, the high capillary suction values observed for air lime mortars are consistent with previous findings in the literature (Forster, 2002). Further details on pore size distribution were plotted Fig. 7.

According to Fig. 7a, the pure cement group (C100L0) exhibited an increase in pores with smaller diameters over time, which was expected due to the progress of hydration and water evaporation. A similar behavior was reported by Olaniyan (2020), who observed that cement-rich mixtures tend to present lower median pore sizes compared to air lime-containing mortars. At later ages, however, a small shift towards larger pores was observed and attributed to the microstructural changes caused by drying stresses and carbonation. For the lime-cement groups shown in Fig. 7b and c, an increase in pores with larger diameters was observed over time. In this case, pores with larger diameters result from (i) moisture depletion caused by the competition between hydration and carbonation, combined with water evaporation; and (ii) the incomplete precipitation of solid phases due to partial hydration and carbonation. These processes disrupt pore continuity, create larger pores, and lead to a less uniform microstructure.

For the pure lime group (C0L100), Fig. 7d did not show significant changes between 28 and 364 days. This behavior reflects air lime's high water retention capacity (also confirmed by Munhoz et al. (2024)) and the slow progression of carbonation under typical environmental conditions, which help limit changes over time. Nevertheless, Fig. 7d shows peaks around 15 μm, 40 μm, and 300 μm, which exceed the typical range reported for air lime mortars (Žižlavský et al., 2021) and most likely correspond to microcracks generated during MIP testing.

For the lime-cement groups shown in Fig. 7b and c, an increase in pores with larger diameters was observed over time. In this case, pores with larger diameters result from (i) moisture depletion caused by the competition between hydration and carbonation, combined with water evaporation; and (ii) the incomplete precipitation of solid phases due to partial hydration and carbonation. These processes disrupt pore continuity, create larger pores, and lead to a less uniform microstructure.

For the pure lime group (C0L100), Fig. 7d did not show significant changes between 28 and 364 days. This behavior reflects air lime's high water retention capacity (also confirmed by Munhoz et al. (2024)) and the slow progression of carbonation under typical environmental conditions, which help limit changes over time. Nevertheless, Fig. 7d shows peaks around 15 μm, 40 μm, and 300 μm, which exceed the typical range reported for air lime mortars (Žižlavský et al., 2021) and most likely correspond to microcracks generated during MIP testing. The low mechanical strength of the pure lime specimens, even at later ages, makes them particularly susceptible to damage under high pressures, such as those applied during MIP testing. This interpretation was also reported by Lanas and Alvarez (2003) and, in this study, is supported by the absence of corresponding large-pore effects in the capillary suction (Fig. 6b) and water absorption (Fig. 5a) results. Hence, the pore size evolution noted in Fig. 7 complements the overall porosity and absorption trends presented in Figs. 5 and 6.

Although a continuous decrease in porosity would typically be expected with the progression of hydration and carbonation, the results shown in Figs. 5 and 6 indicate otherwise. The apparent stabilization trend observed across all mixtures reflects the simultaneous action of

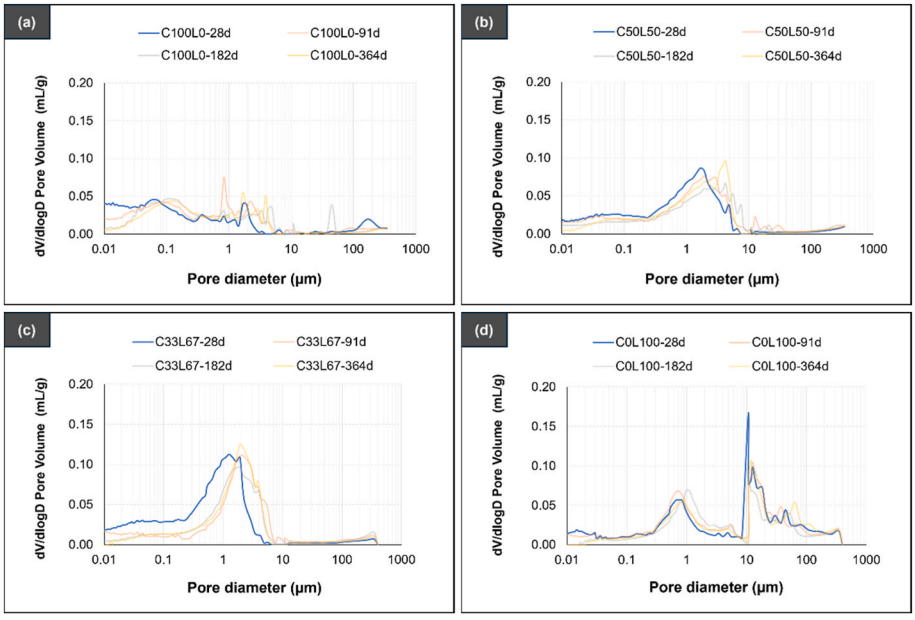

Fig. 7. Pore size distribution for the groups: (a) C100L0; (b) C50L50; (c) C33L67; and (d) C0L100.

multiple competing processes: (i) hydration and carbonation, which contribute to pore refinement through the precipitation of solid phases; (ii) water evaporation and eventual microcracking, which increase overall porosity; and (iii) the high water retention of air lime, which initially regulates both moisture loss and the progress of carbonation. Additionally, according to Lanas and Álvarez (Lanas and Alvarez, 2003), carbonation is a self-limiting process in which the precipitation of $CaCO_3$ progressively reduces permeability, thereby limiting further CO_2 ingress and, consequently, the continuation of carbonation.

Overall, the pore structure evolved differently across mixtures, confirming that the microstructural development of air lime-containing mortars is governed by complex, interdependent mechanisms that require further investigation. These findings also highlight the importance of considering certain methodological aspects when interpreting the results, particularly with regards to open porosity and water absorption, and MIP test conditions.

Open porosity and water absorption tests are typically considered non-destructive. However, for air lime-rich specimens, immersion in water may lead to partial dissolution of uncarbonated $Ca(OH)_2$, particularly at early ages, given its high solubility (approximately 1 g per 630 mL at 25 °C). In such cases, the reuse of specimens is not recommended. In the present study, no evidence of material degradation or mass loss was observed during testing, indicating that the adopted procedure did not significantly affect the results. Nevertheless, this consideration remains relevant for future studies.

Regarding MIP, maintaining consistent boundary conditions is essential. As noted in previous studies (Berodier et al., 2016; Ma, 2014), parameters such as contact angle, pressure range, and equipment configuration (in this study: contact angle 141°; low pressure 0-0.14 MPa; high pressure 0.14-210 MPa) can significantly influence the results. In addition, air lime-rich specimens are particularly susceptible to damage under high intrusion pressures, which may lead to an overestimation of porosity due to microcracking. In the present study, this effect was not found to significantly affect the results; however, it should be carefully considered in future investigations, especially when testing low-strength or early-age air lime mortars.

3.3. Total length change

The total length change test was preceded by an autogenous shrinkage test to assess early-age deformation and provide context for the long-term length change measurements. The autogenous shrinkage results are presented in Fig. 8, where positive values represent expansion and negative values represent shrinkage.

According to Fig. 8a, the pure lime group (C0L100) exhibited significant expansion, attributed to the dissolution and recrystallization of calcium-based phases. This process, known as the lime putty principle, has been previously reported in the literature. Mascolo et al. (2010) observed that, over time, small portlandite crystals tend to gradually dissolve and reprecipitate as larger, more stable ones, leading to a volumetric increase consistent with the expansion recorded in Fig. 8.

A similar but less pronounced trend was also observed in the other air lime-containing groups (C50L50 and C33L67), with the magnitude of expansion decreasing as the lime content in the mixture decreased. Conversely, the pure cement group (C100L0) exhibited low autogenous shrinkage in Fig. 8. This behavior is attributed to the mitigating effect of the limestone addition (CEM II/A-L), which reduces clinker content and enhances particle packing, thereby limiting self-desiccation during cement hydration.

While these results provide insights into the early-age deformation of air lime-containing mortars, certain methodological limitations of the autogenous shrinkage test must be acknowledged. According to ASTM C1698:2019 (American Society for Testing Materials, 2019), the experimental procedure was developed for specimens to be tested under sealed conditions. However, in the case of air lime-containing mortars, sealing prevents the evaporation of excess water and the ingress of CO_2, thereby inhibiting carbonation and hardening. Thus, although the test offers valid information on the early-age behavior of air lime-containing mortars, it does not reflect their deformation behavior under normal curing conditions.

In the hardened state, total length change was measured according to EN 12390-16:2019 (European Committee for Standardization, 2019b), which captures the overall deformation behavior under defined conditions of temperature and relative humidity. Unlike the autogenous shrinkage test, this method does not require sealed conditions and, therefore, provides a more representative assessment of air lime's deformation behavior under typical curing conditions. The results are presented in Fig. 9.

According to Fig. 9, most length changes occurred within 91 days after casting, followed by a stabilization trend. For the pure lime group (C0L100), two mechanisms explain the observed expansion: (i) air lime's high water retention capacity, which regulates moisture loss and mitigates drying stresses associated with water evaporation; and (ii) the expansive nature of carbonation, as the conversion of $Ca(OH)_2$ to $CaCO_3$ results in a theoretical volumetric expansion of about 11.6 %. In contrast, the self-limiting nature of carbonation explains the stabilization trend observed at later ages. As carbonation progresses, $CaCO_3$ precipitates fill superficial pores, hindering further ingress of CO_2 and gradually restricting long-term carbonation.

The lime-cement groups (C50L50 and C33L67) exhibited the most pronounced expansion, as shown in Fig. 9. Differently from the pure

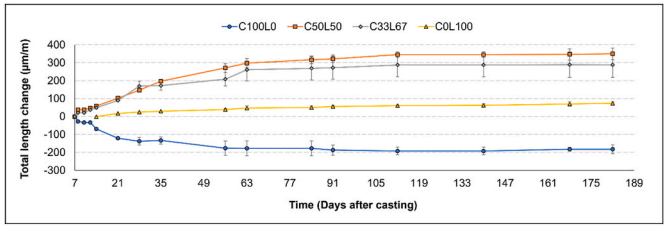

Fig. 9. Total length change of C100L0, C50L50, C33L67, and C0L100 up to 182 days.

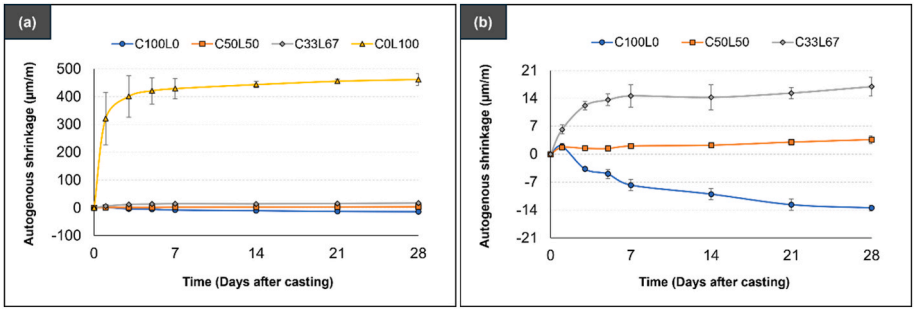

Fig. 8. Shrinkage behavior: (a) autogenous shrinkage and (b) autogenous shrinkage results zoomed-in, excluding C0L100.

lime group (C0L100), this behavior results from the competition for available moisture, which accelerates pore desaturation (through water evaporation or consumption during cement hydration) and enables earlier and more extensive carbonation. The competition for moisture in lime-cement mortars was extensively studied by Cizer (2009) and colleagues (Cizer et al., 2010, 2012). Hence, the precipitation of $CaCO_3$ contributes to the expansive behavior recorded. At later ages, depleted moisture levels and the self-limiting nature of carbonation explain the stabilization trend observed in Fig. 9. No statistical difference was found between C50L50 and C33L67.

Contrary to the air lime-containing groups, the pure cement specimens (C100L0) exhibited shrinkage. According to Fig. 9, most of the length change occurred immediately after the monitoring started, suggesting that moisture loss was the main mechanism behind the observed shrinkage. The stabilization trend recorded at later ages supports this interpretation, indicating that the specimens reached moisture equilibrium with the environment.

Overall, the length change behavior reflects the interplay between shrinkage (caused by water evaporation and the carbonation of hydrated phases (Ramesh, 2021)) and expansion (resulting from $CaCO_3$ precipitation, which can overcompensate the shrinkage tendency, as reported in (Swenson and Sereda, 1968)). Moreover, the stabilization trend observed after 112 days does not indicate complete hydration or carbonation but rather suggests that (i) limited moisture availability restricts further hydration and carbonation reactions; and (ii) pore clogging by $CaCO_3$ precipitates progressively limits further CO_2 ingress and carbonation.

In addition to the methodological limitations previously discussed, the influence of specimen size should also be considered. According to Zhang and Hubler (2020), smaller specimens tend to exhibit greater shrinkage strains than larger ones due to their higher surface-to-volume ratio, which accelerates drying and directly affects the rates of water evaporation, hydration, and carbonation. Therefore, proper documentation of specimen dimensions and boundary conditions is essential to enable FAIR-based comparisons.

3.4. Compressive strength

The compressive strength results for the four mortar groups are presented in Fig. 10 and indicate that increasing the air lime content leads to a reduction in compressive strength. This trend has been consistently observed in the literature (Kang et al., 2019; Pavia et al., 2019; Ramesh, 2021; Macharia, 2015) and is attributed to the distinct mechanisms of cement hydration and air lime carbonation. Portland cement primarily relies on the hydration of alite (C_3S) and belite (C_2S) to form calcium silicate hydrate (C-S-H), which produces a dense and cohesive matrix. In contrast, air lime mortars rely on the carbonation of calcium-based phases for microstructural development. However, $CaCO_3$ lacks the dense, interlocking microstructure characteristic of C–S–H, which helps explain air lime's lower compressive strength compared with Portland cement mortars. This interpretation aligns with findings reported in the literature (Li et al., 2020; Manzano et al., 2012).

Additional factors limiting the strength development of the pure lime group (C0L100) include (i) the low CO_2 concentration under normal atmospheric conditions, which is about 400 ppm (0.04 % CO_2); and (ii) the fact that carbonation can only occur after the excess water has evaporated, leaving pores unsaturated and allowing CO_2 to diffuse into the microstructure. Hence, as widely reported in the literature (Kang et al., 2019; Cizer, 2009), carbonation is a slow process, particularly at early ages.

According to Fig. 10, an increase in strength was observed between 28 and 91 days, reflecting the ongoing hydration and carbonation processes. After 91 days, however, a stabilization trend was recorded for all groups, except C0L100. This behavior confirms the slow nature of carbonation, which progressively increases strength over time. Additionally, for the pure cement group (C100L0), a decreasing trend was observed between 91 and 364 days and is associated with microcracking caused by shrinkage. This interpretation is consistent with the MIP curves and length change results shown in Figs. 7a and 9, respectively.

For lime-cement mortars, Cizer (2009) suggested that an interaction between hydration and carbonation may occur under low relative humidity conditions (i.e., 55 % RH). Therefore, in this context, the water retention capacity of air lime is expected to retain moisture, prolonging cement hydration, which promotes pore desaturation, enabling the ingress of CO_2 and favoring carbonation. However, compressive strength measurements alone are insufficient to confirm this interaction. Therefore, additional experiments (mass monitoring, phenolphthalein spraying, and thermogravimetric analysis) were conducted.

3.5. Additional experiments

The interaction between hydration and carbonation was further investigated through mass monitoring, carbonation depth using phenolphthalein, and TGA. The results are discussed in the next subsections.

3.5.1. Mass monitoring

The four mortar groups were continuously monitored for mass variation, and the results are presented in Fig. 11. The pure lime group (C0L100) consistently exhibited a positive mass change, confirming that the carbonation of air lime is an expansive process in terms of both length change and mass gain. In contrast, the air lime-cement groups (C50L50 and C33L67) exhibited the highest mass loss.

According to Fig. 11, C50L50 and C33L67 exhibited significant mass losses up to 28 days after casting, which are attributed to a change in environmental conditions. During the first 7 days after casting, the specimens were cured at 95 % RH, in accordance with EN 1015-11:2019 (European Committee for Standardization, 2019a). They were then transferred to a 55 % RH environment, in accordance with EN 12390-16:2019 (European Committee for Standardization, 2019b). As a result, the reduction in relative humidity created a moisture gradient between the specimens and the environment, causing water to evaporate from the specimens and explaining the mass losses observed for the lime-cement groups.

The early-age mass losses also indicate that the high initial water content and increased porosity of the lime-cement groups facilitated moisture transport. At later ages, however, stabilization and a gradual mass increase were recorded for C50L50 and C33L67, respectively,

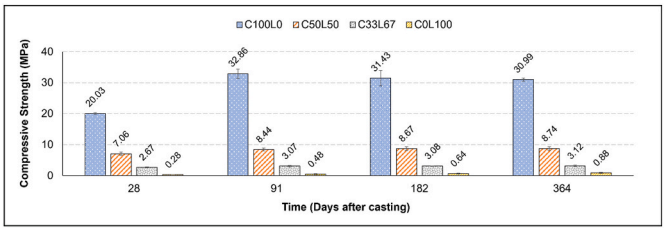

Fig. 10. Compressive strength of cubic specimens.

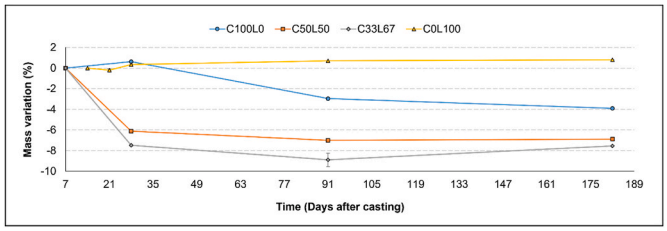

Fig. 11. Mass evolution up to 182 days.

which can be attributed to the specimens reaching moisture equilibrium with the environment and the progressive precipitation of $CaCO_3$ during carbonation.

For the pure cement group (C100L0), a similar trend was observed. In this case, the specimens were cured at 95 % RH for 28 days and then transferred to a 55 % RH environment for testing, following EN 12390-16:2019 (European Committee for Standardization, 2019b). Hence, during the first 28 days after casting, the specimens exhibited mass gain consistent with the continuous hydration of Portland cement. After that, a mass decrease was recorded, driven by the moisture gradient between the specimens and the environment. Similar results were reported in the literature (Kang et al., 2019; Pavlík and Užáková, 2016).

Overall, these findings are consistent with Kang et al. (2019), who reported that lime-containing mortars undergo simultaneous CO_2 uptake and water evaporation, with the rate of evaporation having a decisive influence on the overall mass change.

3.5.2. Carbonation depth using phenolphthalein

At the end of the total length change test, the specimens were split in half and phenolphthalein was sprayed onto their fractured surfaces. The results are presented in Fig. 12.

After 182 days, C100L0, C50L50, C33L67, and C0L100 exhibited carbonation depths of 0.4 mm, 17 mm, 24 mm, and 32 mm, respectively. These results indicate that mixtures with higher air lime contents experienced more extensive carbonation, consistent with findings reported in the literature (Kang et al., 2019; Branco et al., 2021). This behavior is attributed to two complementary factors: air lime's specific surface area and its chemical composition.

Air lime is known for its high specific surface area (Table 3). Consequently, mixtures with higher air lime contents required more water to achieve the same workability level as those with lower air lime contents. During storage, however, this excess water either evaporated or was consumed through continued cement hydration, leaving behind a porous matrix. As a result, CO_2 ingress and subsequent carbonation were facilitated.

Moreover, air lime's chemical composition consists primarily of $Ca(OH)_2$, which is highly reactive with CO_2. Therefore, mixtures with higher air lime contents provided a greater availability of $Ca(OH)_2$ which, under favorable environmental conditions, led to the greater carbonation extents observed in air lime-rich mortars (Fig. 12).

According to Fig. 12, a distinctive behavior was observed for the pure lime group (C0L100) and, to a lesser extent, for the lime-cement groups (C50L50 and C33L67). After spraying the phenolphthalein indicator, the carbonation front was initially revealed. However, shortly after spraying the phenolphthalein solution, the entire fractured surface of the specimens exhibited varying shades of pink. According to Romero-Hermida et al. (2021) varying shades of pink may appear when carbonated and uncarbonated phases coexist. Therefore, two hypotheses were formulated to explain this phenomenon: (i) the high pH of the specimens, and (ii) the formation of Liesegang rings.

The first hypothesis suggests that the pH of the specimens remained highly alkaline (pH > 9) despite ongoing carbonation. Consequently, the overall pH reduction associated with carbonation was not sufficient to be detected by the phenolphthalein indicator. Air lime is known for its high alkalinity, which supports this interpretation.

The second hypothesis concerns the formation of Liesegang rings. In this case, localized patterns created by gradients in moisture levels, concentration of calcium-based phases, or physical discontinuities in the pore network promote the carbonation of $Ca(OH)_2$ at specific locations while hindering it at adjacent ones. This mechanism explains the presence of irregular pink stains (uncarbonated phases) within the carbonated layer. Further details on Liesegang ring formation are available in (Rodriguez-Navarro et al., 2002).

To further understand the distinctive behavior observed in the air-lime containing groups shown in Fig. 12, TGA was performed. This analysis allows comparison with the phenolphthalein results, providing complementary evidence of the carbonation behavior observed in the specimens.

3.5.3. Thermogravimetric analysis (TGA)

The TGA results of the four mortar mixtures revealed the coexistence of $Ca(OH)_2$ and $CaCO_3$ phases at all analyzed ages. The corresponding plots are presented in Fig. 13 with differential TGA (DTGA) curves. The choice for DTGA facilitates the distinction of different phases through the whole temperature range, and the individual peaks were identified according to the recommendations of Lothenbach et al. (2016). Similar patterns were reported in previous studies (Kang et al., 2019; Arizzi et al., 2013).

Three characteristic peaks were identified in Fig. 13, occurring at approximately 150, 450, and 750 °C. The first peak (~150 °C) is associated with phases derived from Portland cement hydration, such as gypsum, C–S–H, ettringite, and monocarbonates (Lothenbach et al., 2016). As expected, this peak was more pronounced in mixtures with higher cement contents and disappeared entirely in the pure lime group (C0L100). Nonetheless, mass loss was still observed in C0L100 between 40 and 400 °C, which is attributed to the evaporation of bound water.

The second peak (~450 °C) corresponds to $Ca(OH)_2$ (Lothenbach et al., 2016). According to Fig. 13, these peaks decreased over time, reflecting the progressive consumption of $Ca(OH)_2$ during the carbonation reactions.

The third peak (600–800 °C) is attributed to $CaCO_3$, and the increase of this peak over time is consistent with the carbonation depth results, confirming the progressive precipitation of $CaCO_3$. The precipitation of $CaCO_3$ may include polymorphs such as vaterite and aragonite (Lothenbach et al., 2016). However, since these polymorphs have comparable molecular masses, they cannot be distinguished through DTGA. Complementary techniques, such as SEM/EDX, NMR, or Raman spectroscopy, are recommended to identify them.

When interpreting the results from Fig. 13, two considerations must be noted. First, the TG analyses were conducted on mortar samples containing siliceous sand. Although it is known that siliceous aggregates are inert and have a negligible influence on the TGA results (Oliveira et al., 2017), their presence can still affect quantitative estimations. Conducting TGA at the paste level was considered impractical because the results would not be directly comparable to the carbonation extent at the mortar level, as reported by Cizer (2009). The differences between paste-mortar levels arise from the influence of aggregates on the microstructure, particularly affecting the interfacial transition zone,

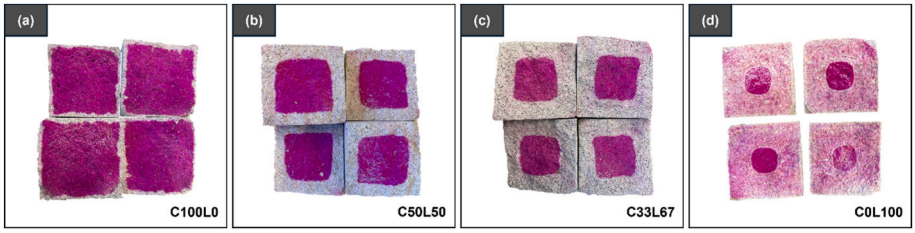

Fig. 12. Phenolphthalein stains on the (a) C100L0, (b) C50L50, (c) C33L67, (d) C0L100 total length change specimens at 182 days.

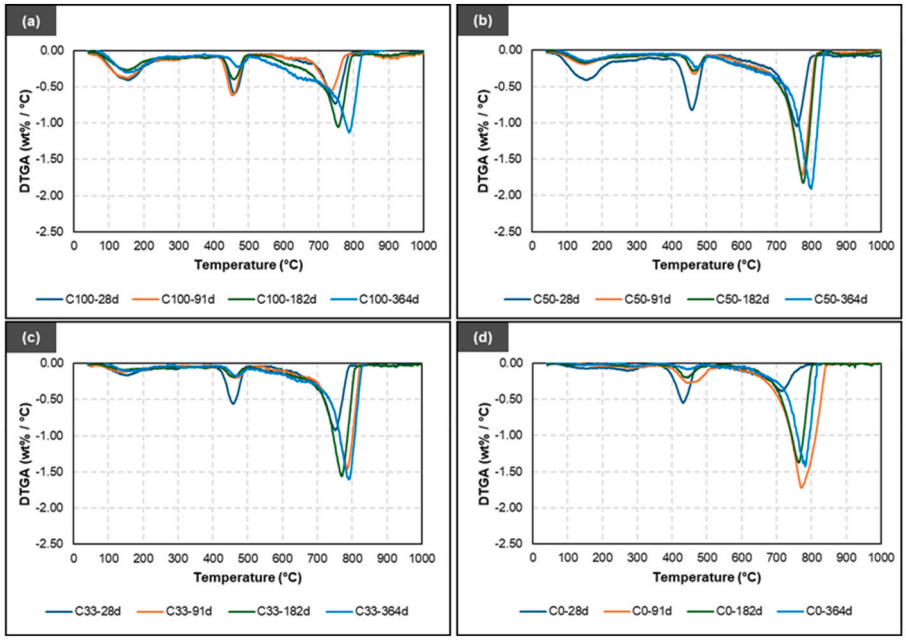

Fig. 13. Thermogravimetric analysis of (a) C100L0; (b) C50L50; (c) C33L67; and (d) C0L100.

pore network, and transport properties. Second, the cement used in this study (CEM II/A-L 32.5R) contains limestone filler ($CaCO_3$), which may have led to an overestimation of the carbonated phases, particularly in mixtures with higher cement content. In this case, the TGA of the cement powder was performed, and the CO_2 released during its decarbonation was normalized to the cement fraction of each mixture and subsequently subtracted from the corresponding mortar results.

The semi-quantitative analysis of the TGA, plotted shown in in Fig. 14, show the results grouped into three main temperature ranges: (i) 40-400 °C, corresponding to the loss of free and bound water, as well as the dehydration of cementitious phases; (ii) 400-500 °C, attributed to the dehydroxylation of $Ca(OH)_2$; and (iii) 500-1100 °C, related to the decarbonation of $CaCO_3$ (excluding limestone filler).

Overall, the weight loss associated with calcium carbonate decarbonation increased over time in all mixtures, confirming the progressive nature of carbonation. Conversely, the mass loss linked to $Ca(OH)_2$ dehydroxylation decreased more slowly in the Portland cement group (C100L0) and remained relatively constant after 91 days in the air lime-containing groups, indicating that a considerable $Ca(OH)_2$ reserve persisted due to the slow progression of carbonation under ambient conditions and the high lime availability in these groups. Finally, the weight loss between 40 and 400 °C can be attributed to the carbonation of cementitious hydrates (i.e., Fig. 14a) and to the evaporation of free and bound water, particularly in air lime-containing mortars, where air lime's high water retention capacity limits moisture loss at ambient temperatures.

In summary, the TGA results provide complementary evidence of the slow yet continuous carbonation process in air lime-containing mortars,

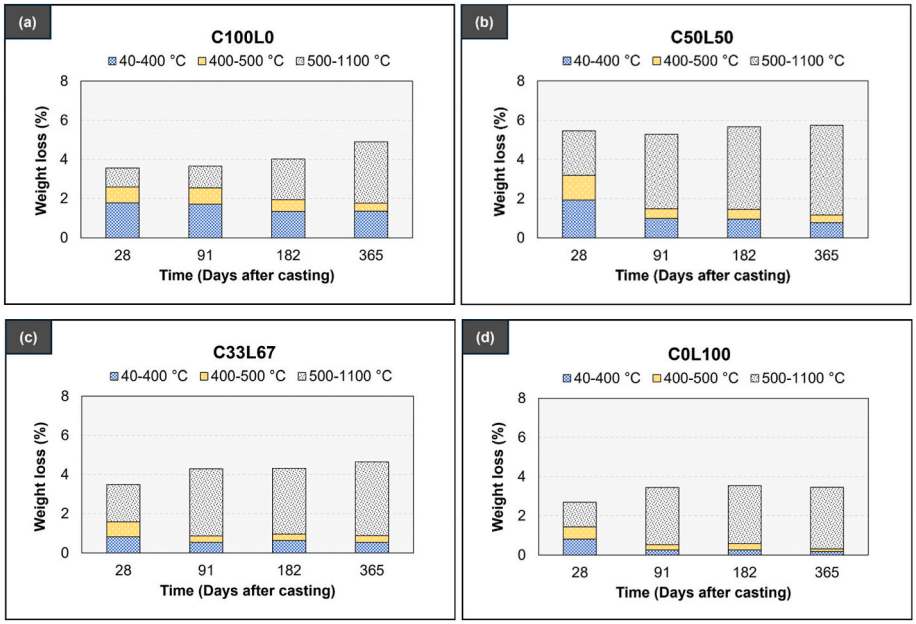

Fig. 14. Normalized TGA results excluding the CO_2 contribution from the added limestone.

supporting the observations from the physical and chemical characterizations.

4. Conclusions

This study aimed to support the transition toward more transparent and reproducible research practices in the field of air lime by combining experimental characterization with a FAIR-aligned workflow. In this context, four air lime-containing mortar mixtures were monitored for up to 12 months, and datasets on fresh properties (entrapped air content and setting times), physical properties (pore structure, total length change, and mass evolution), and mechanical performance (compressive strength) were made openly accessible through a trusted repository. The experimental program conducted in this work thus served both to characterize material behavior under clearly defined conditions and to demonstrate how FAIR and reproducible research practices can be implemented in lime mortar studies. The main conclusions are summarized in sequence.

- **Fresh properties:** Mixtures with higher air lime contents exhibited longer initial and final setting times. They primarily depend on drying and carbonation for microstructural development, which takes time and is particularly sensitive to relative humidity. Additionally, at the fresh state, air lime-rich mixtures showed lower entrapped air contents, as lime particles are small and have a physical filler effect.
- **Pore structure:** At the hardened state, air lime-rich mixtures exhibited higher open porosity and water absorption. This was attributed to (i) the slow carbonation of lime; (ii) the evaporation of the excess water; and (iii) the intrinsic porosity of air lime. Moreover, the MIP pressures can damage air lime-containing mortars and overestimate their total porosity. A direct relationship between air lime content and capillary suction could not be established.
- **Total length change:** The autogenous shrinkage test conditions were unsuitable for air lime mortars. In contrast, the total length change test showed that air lime-containing mortars exhibited expansion, while the pure cement mixture exhibited shrinkage. This behavior was attributed to the expansive nature of the carbonation reactions of air lime and the curing conditions, respectively.
- **Competition for moisture:** In lime-cement mortars, the competition for moisture between cement hydration, air lime carbonation, and water evaporation accelerated pore desaturation and enabled earlier and more extensive carbonation. Air lime's high water retention capacity also prolonged cement's hydration, explaining the outcomes observed in the characterization of the pore structure and total length change.
- **Compressive strength and carbonation depth:** Increasing air lime content led to a reduction in compressive strength, indicating that the strength development of air lime-rich mixtures was limited by the low CO_2 concentration under ambient conditions and the excess pore water, which delayed the carbonation process. Moreover, the carbonation depth was proportional to the air lime content in the mixtures.
- **Mass monitoring:** Lime-cement mortars (C50L50 and C33L67) showed significant mass losses due to the moisture gradient between the specimens and the environment. In contrast, the pure lime mixture (C0L100) gained mass through carbonation, confirming its expansive nature.
- **Carbonation monitoring:** Phenolphthalein tests revealed varying shades of pink, particularly in air lime-rich mixtures, which were attributed to high specimen alkalinity and possible Liesegang ring formation. TGA results confirmed the coexistence of $Ca(OH)_2$ and $CaCO_3$ phases, showing a decrease in $Ca(OH)_2$ peaks and an increase in $CaCO_3$ peaks over time, consistent with progressive carbonation.

In summary, the results indicate that air lime content influences not only individual mechanisms but also coupled responses. For instance, mixtures with higher lime contents exhibited increased porosity and higher water retention, which in turn influenced carbonation kinetics, dimensional changes, and strength development. Additionally, in blended lime-cement systems, interactions due to the competition for moisture between cement hydration, carbonation, and moisture evaporation were observed. These interdependencies highlight the importance of considering mixture composition, moisture transport, and carbonation processes simultaneously when evaluating air lime-containing mortars.

CRediT authorship contribution statement

Guilherme da Silva Munhoz: Conceptualization, Data curation, Formal analysis, Investigation, Methodology, Visualization, Writing – original draft, Writing – review & editing. **Yu Zeng:** Formal analysis, Writing – review & editing. **Luiz Miranda de Lima Junior:** Formal analysis, Investigation, Writing – review & editing. **Guang Ye:** Conceptualization, Funding acquisition, Methodology, Project administration, Supervision, Writing – review & editing.

Declaration of competing interest

The authors declare that they have no known competing financial interests or personal relationships that could have appeared to influence the work reported in this paper.

Acknowledgments

This research has been carried out within the framework of the EU SUBLime network. This Project has received funding from the European Union's Horizon 2020 research and innovation programme under Marie Sklodowska-Curie project SUBLime [Grant Agreement n∘955986].

Data availability

Research link to be provided. Datasets available in an OA repository.

References

Alvarez, J.I., Veiga, R., Martínez-Ramírez, S., Secco, M., Faria, P., Maravelaki, P.N., Ramesh, M., Papayianni, I., Válek, J., 2021. RILEM TC 277-LHS report: a review on the mechanisms of setting and hardening of lime-based binding systems. Mater. Struct. 54 (2), 63. https://doi.org/10.1617/S11527-021-01648-3.

American Society for Testing Materials, 2017. ASTM C403: Standard Test Method for Time of Setting of Concrete Mixtures by Penetration Resistance. West Conshohocken.

American Society for Testing Materials, 2019. C1698: Standard Test Method for Autogenous Strain of Cement Paste and Mortar. West Conshohocken.

American Society for Testing Materials, 2020. ASTM C185: Standard Test Method for Air Content of Hydraulic Cement Mortar. West Conshohocken.

American Society for Testing Materials, 2021. ASTM C191: Standard Test Methods for Time of Setting of Hydraulic Cement by Vicat Needle. West Conshohocken.

Arandigoyen, M., Bernal, J.L.P., López, M.A.B., Alvarez, J.I., 2005. Lime-pastes with different kneading water: pore structure and capillary porosity. Appl. Surf. Sci. 252, 1449–1459. https://doi.org/10.1016/j.apsusc.2005.02.145.

Arandigoyen, M., Alvarez, J.I., 2007. Pore structure and mechanical properties of cement–lime mortars. Cement Concr. Res. 37, 767–775. https://doi.org/10.1016/j.cemconres.2007.02.023.

Arizzi, A., Cultrone, G., 2013. Negative effects of the use of white Portland cement as additive to aerial lime mortars set at atmospheric conditions: a chemical, mineralogical and physical-mechanical investigation. In: Rivera, S.M., Diaz, A.L.P. (Eds.), Brick and Mortar Research, first ed. Nova Science Publishers, pp. 231–243.

Arizzi, A., Cultrone, G., 2013. The influence of aggregate texture, morphology and grading on the carbonation of non-hydraulic (aerial) limebased mortars. Q. J. Eng. Geol. Hydrogeol. 46, 507–520. https://doi.org/10.1144/QJEGH2012-017.

Associação Brasileira de Normas Técnicas, 2005. NBR 9778: Hardened Mortar and Concrete - Determination of Absorption, Voids and Specific Gravity. Rio de Janeiro.

Ball, R.J., El-Turki, A., Allen, G.C., 2011. Influence of carbonation on the load dependent deformation of hydraulic lime mortars. Mater. Sci. Eng., A 528, 3193–3199. https://doi.org/10.1016/J.MSEA.2010.12.070.

Berodier, E., Bizzozero, J., Muller, A.C.A., 2016. Mercury intrusion porosimetry. In: Scrivener, K., Snellings, R., Lothenbach, B. (Eds.), A Practical Guide to Microstructural Analysis of Cementitious Materials, first ed. CRC Press, Boca Raton.

Branco, F.G., Belgas, M. de L., Mendes, C., Pereira, L., Ortega, J.M., 2021. Characterization of fresh and durability properties of different lime mortars for being used as masonry coatings in the restoration of ancient constructions. Sustainability 13, 4909. https://doi.org/10.3390/SU13094909.

Carran, D., Hughes, J., Leslie, A., Kennedy, C., 2012. A short history of the use of lime as a building material beyond Europe and North America. Int. J. Architect. Herit. 6, 117–146. https://doi.org/10.1080/15583058.2010.511694.

Cizer, O., 2009. Competition Between Carbonation and Hydration on the Hardening of Calcium Hydroxide and Calcium Silicate Binders. Katholieke Universiteit Leuven. Doctoral thesis.

Cizer, Ö., Van Balen, K., Elsen, J., Van Gemert, D., 2012. Real-time investigation of reaction rate and mineral phase modifications of lime carbonation. Constr. Build. Mater. 35, 741–751. https://doi.org/10.1016/J.CONBUILDMAT.2012.04.036.

Cizer, Ö., Van Balen, K., Van Gemert, D., 2010. Competition between hydration and carbonation in hydraulic lime and lime-pozzolana mortars. Adv. Mater. Res. 133–134, 241–246. https://doi.org/10.4028/WWW.SCIENTIFIC.NET/AMR.133-134.241.

da Silva Munhoz, G., Ye, G., 2025. Creep in carbonatable binders: investigating non-hydraulic lime mortars. Constr. Build. Mater. 496, 143751. https://doi.org/10.1016/J.CONBUILDMAT.2025.143751.

de Medeiros-Junior, R.A., Munhoz, G. da S., de Medeiros, M.H.F., 2019. Correlations between water absorption, electrical resistivity and compressive strength of concrete with different contents of pozzolan. Revista ALCONPAT 9, 152–166. https://doi.org/10.21041/RA.V9I2.335.

Dheilly, R.M., Tudo, J., Sebaibi, Y., Quéneudec, M., 2002. Influence of storage conditions on the carbonation of powdered Ca(OH)2. Constr. Build. Mater. 16, 155–161. https://doi.org/10.1016/S0950-0618(02)00012-0.

European Commission, The European green deal - european commission, (n.d.). https://commission.europa.eu/strategy-and-policy/priorities-2019-2024/european-green-deal_en (accessed July 14, 2025).

European Committee for Standardization, 2003. EN 1015-18 Methods of Test for Mortar for Masonry – Part 18: Determination of Water Absorption Coefficient due to Capillary Action of Hardened Mortar. Brussels.

European Committee for Standardization, 2015. EN 459-1 Building Lime - Part 1: Definitions, Specifications and Conformity Criteria. Brussels.

European Committee for Standardization, 2016. EN 196-1: Methods of Testing Cement – Part 1. Determination of strength, Brussels.

European Committee for Standardization, 2021. EN 459-2: Building Lime - Part 2: Test Methods. Brussels.

European Committee for Standardization, 1998a. EN 1015-1: Methods of Test for Mortar for Masonry - Part 1: Determination of Particle Size Distribution (By Sieve Analysis). Brussels.

European Committee for Standardization, 2019a. EN 1015-11: Methods of Test for Mortar for Masonry - Part 11: Determination of Flexural and Compressive Strength of Hardened Mortar. Brussels.

European Committee for Standardization, 1998b. EN 1015-6: Methods of Test for Mortar for Masonry - Part 6: Determination of Bulk Density of Fresh Mortar. Brussels.

European Committee for Standardization, 2019b. EN 12390-16: Testing Hardened Concrete - Part 16: Determination of the Shrinkage of Concrete. Brussels.

European Committee for Standardization, 2019c. EN 12390-3: Testing Hardened Concrete - Part 3: Compressive Strength of Test Specimens. Brussels.

Forster, A.M., 2002. An Assessment of the Relationship Between the Water Vapour Permeability and Hydraulicity of Lime-based Mortars with Particular Reference to Building Conservation Materials Science, Doctoral Thesis. Heriot-Watt University.

Fourmentin, M., Ovarlez, G., Faure, P., Peter, U., Lesueur, D., Daviller, D., Coussot, P., 2015. Rheology of lime paste—a comparison with cement paste. Rheol. Acta 54 (7), 647–656. https://doi.org/10.1007/S00397-015-0858-7.

Groot, C., Veiga, R., Papayianni, I., Van Hees, R., Secco, M., Alvarez, J.I., Faria, P., Stefanidou, M., 2022. RILEM TC 277-LHS report: lime-based mortars for restoration–a review on long-term durability aspects and experience from practice. Mater. Struct. 55 (10), 245. https://doi.org/10.1617/S11527-022-02052-1.

Hansen, E.F., Rodríguez-Navarro, C., Van Balen, K., 2008. Lime putties and mortars. Stud. Conserv. 53, 9–23. https://doi.org/10.1179/SIC.2008.53.1.9.

Žižlavský, T., Bayer, P., Vyšvařil, M., 2021. Bond properties of NHL-based mortars with viscosity-modifying water-retentive admixtures. Minerals 11, 685. https://doi.org/10.3390/MIN11070685.

Kang, S.H., Kwon, Y.H., Moon, J., 2019. Quantitative analysis of CO2 uptake and mechanical properties of air lime-based materials. Energies 12, 2903. https://doi.org/10.3390/EN12152903.

Lanas, J., Bernal, J.L.P., Bello, M.A., Galindo, J.I.A., 2004. Mechanical properties of natural hydraulic lime-based mortars. Cement Concr. Res. 34, 2191–2201. https://doi.org/10.1016/J.CEMCONRES.2004.02.005.

Lanas, J., Sirera, R., Alvarez, J.I., 2005. Compositional changes in lime-based mortars exposed to different environments. Thermochim. Acta 429, 219–226. https://doi.org/10.1016/J.TCA.2005.03.015.

Lanas, J., Alvarez, J.I., 2003. Masonry repair lime-based mortars: factors affecting the mechanical behavior. Cement Concr. Res. 33, 1867–1876. https://doi.org/10.1016/S0008-8846(03)00210-2.

Lawrence, R.M., Mays, T.J., Rigby, S.P., Walker, P., D'Ayala, D., 2007. Effects of carbonation on the pore structure of non-hydraulic lime mortars. Cement Concr. Res. 37, 1059–1069. https://doi.org/10.1016/J.CEMCONRES.2007.04.011.

Li, B., Li, N., Brouwers, H.J.H., Yu, Q., Chen, W., 2020. Understanding hydrogen bonding in calcium silicate hydrate combining solid-state NMR and first principle calculations. Constr. Build. Mater. 233, 117347. https://doi.org/10.1016/J.CONBUILDMAT.2019.117347.

Liu, Z., Lv, C., Wang, F., Hu, S., 2023. Recent advances in carbonatable binders. Cement Concr. Res. 173, 107286. https://doi.org/10.1016/J.CEMCONRES.2023.107286.

Lothenbach, B., Durdziński, P., De Weerdt, K., 2016. Thermogravimetric analysis. In: Scrivener, K., Snellings, R., Lothenbach, B. (Eds.), A Practical Guide to Microstructural Analysis of Cementitious Materials, first ed. CRC Press, Boca Raton.

Ma, H., 2014. Mercury intrusion porosimetry in concrete technology: tips in measurement, pore structure parameter acquisition and application. J. Porous Mater. 21, 207–215. https://doi.org/10.1007/S10934-013-9765-4/FIGURES/10.

Macharia, S.M., 2015. Creep Mechanisms in Cement and Lime Mortared Masonry. University of Bath. Doctoral thesis.

Manzano, H., Moeini, S., Marinelli, F., Van Duin, A.C.T., Ulm, F.J., Pellenq, R.J.M., 2012. Confined water dissociation in microporous defective silicates: mechanism, dipole distribution, and impact on substrate properties. J. Am. Chem. Soc. 134, 2208–2215. https://doi.org/10.1021/JA209152N/SUPPL_FILE/JA209152N_SI_002.MPG.

Maravelaki, P.-N., Kapetanaki, Kali, Papayianni, Ioanna, Ioannou, Ioannis, Faria, Paulina, Alvarez, Jose, Stefanidou, Maria, Nunes, Cristiana, Theodoridou, Magdalini, Ferrara, Liberato, Toniolo, Lucia, Maravelaki, N., Kapetanaki, K., Papayianni, I., Ioannou, I., Faria, P., Alvarez, J., Stefanidou, M., Nunes, C., Theodoridou, M., Ferrara, L., Toniolo, L., Alvarez, J.I., Arizzi, A., Bicer-Simsir, B., Bokan-Bosiljkov, V., Carneiro, A.M., Brito De Carvalho, C., Groot, C., Gulotta, D., Hughes, J.J., Kim, H., Kyriakou, L., Lara Nunes, C., Maravelaki, P.-N., Martinez-Ramirez, S., Oktay, D., Pachta, V., Padovnik, A., Pasian, C., Pavia, S., Pesce, G., Peter, U., Ramesh, M., Rani, D., Pradeep Saridhe, S., Secco, M., Stukovnik, P., Tedeschi, C., Valek, J., van Hees, R., Rosario Veiga P-N Maravelaki, M., Kapetanaki, Á.K., Papayianni Á Stefanidou, I.M., Faria, P., Alvarez, J., Nunes, C., Theodoridou, M., 2023. RILEM TC 277-LHS report: additives and admixtures for modern lime-based mortars. Mater. Struct. 56 (5), 106. https://doi.org/10.1617/S11527-023-02175-Z.

Mascolo, G., Mascolo, M.C., Vitale, A., Marino, O., 2010. Microstructure evolution of lime putty upon aging. J. Cryst. Growth 312, 2363–2368. https://doi.org/10.1016/J.JCRYSGRO.2010.05.020.

Mehta, P.K., Monteiro, P.J.M., 2006. In: Concrete – Microstructure, Properties and Materials, third ed. McGraw Hill, New York.

Munhoz, G.S., Zeng, Y., Schlangen, E., Ye, G., 2024. The water retention role in the carbonation of air lime: hero or villain? In: Lourenço, P.B., Azenha, M., Pereira, J.M. (Eds.), Towards the next Generation of Sustainable Masonry Systems: Mortars, Renders, Plasters and Other Challenges. Universidade do Minho, Funchal, pp. 71–72.

Olaniyan, S.A., 2020. Impact of changing microstructural compositions of lime based mortar on flexibility: case study of sustainable lime-cement composites, advances in science. Technol Eng. Sys. 5, 1488–1498. https://doi.org/10.25046/AJ0506179.

Oliveira, M.A., Azenha, M., Lourenço, P.B., Meneghini, A., Guimarães, E.T., Castro, F., Soares, D., 2017. Experimental analysis of the carbonation and humidity diffusion processes in aerial lime mortar. Constr. Build. Mater. 148, 38–48. https://doi.org/10.1016/j.conbuildmat.2017.04.120.

Pachta, Vasiliki, Stefanidou, Maria, Konopisi, Stavroula, Papayianni, Ioanna, 2014. Technological evolution of historic structural mortars. J. Civil Eng. Architect. 8. https://doi.org/10.17265/1934-7359/2014.07.005.

Pavía, S., Aly, M., 2016. Influence of aggregate and supplementary cementitious materials on the properties of hydrated lime (CL90s) mortars. Mater. Construcción 66, e104. https://doi.org/10.3989/MC.2016.01716.

Pavía, S., Treacy, E., 2006. A comparative study of the durability and behaviour of fat lime and feebly-hydraulic lime mortars. Mater Struct. Materiaux et Construct. 39, 391–398. https://doi.org/10.1617/S11527-005-9033-4/METRICS.

Pavia, S., Brennan, O., 2019. Portland cement-lime mortars for conservation. In: Hughes, J.J., Válek, J., Groot, C.J.W.P. (Eds.), Historic Mortars, first ed. Springer, Cham, pp. 129–142. https://doi.org/10.1007/978-3-319-91606-4_10.

Pavlík, V., Užáková, M., 2016. Effect of curing conditions on the properties of lime, lime–metakaolin and lime–zeolite mortars. Constr. Build. Mater. 102, 14–25. https://doi.org/10.1016/J.CONBUILDMAT.2015.10.128.

Ramesh, M., 2021. A Multi Scale Approach to the Study of lime-cement Mortars in Masonry. Universidade do Minho. Doctoral thesis.

Rodriguez-Navarro, C., Cazalla, O., Elert, K., Sebastian, E., 2002. Liesegang pattern development in carbonating traditional lime mortars. Proceed. Royal Soc. London. Ser. A: Math. Phys. Eng. Sci. 458, 2261–2273. https://doi.org/10.1098/RSPA.2002.0975.

Rodriguez-Navarro, C., Ilić, T., Ruiz-Agudo, E., Elert, K., 2023. Carbonation mechanisms and kinetics of lime-based binders: an overview. Cement Concr. Res. 173, 107301. https://doi.org/10.1016/J.CEMCONRES.2023.107301.

Romero-Hermida, M.I., Borrero-López, A.M., Flores-Alés, V., Alejandre, F.J., Franco, J. M., Santos, A., Esquivias, L., 2021. Characterization and analysis of the carbonation process of a lime mortar obtained from phosphogypsum waste. Int. J. Environ. Res. Publ. Health 18, 6664. https://doi.org/10.3390/IJERPH18126664.

Roy, S.K., Poh, K.B., Northwood, D.O., 1999. Durability of concrete—accelerated carbonation and weathering studies. Build. Environ. 34, 597–606. https://doi.org/10.1016/S0360-1323(98)00042-0.

Ruiz-Agudo, E., Rodriguez-Navarro, C., 2009. Microstructure and rheology of Lime putty. Langmuir 26, 3868–3877. https://doi.org/10.1021/LA9034030Z.

Santos, A.R., Veiga, M. do R., Santos Silva, A., de Brito, J., Álvarez, J.I., 2018. Evolution of the microstructure of lime based mortars and influence on the mechanical behaviour: the role of the aggregates. Constr. Build. Mater. 187, 907–922. https://doi.org/10.1016/J.CONBUILDMAT.2018.07.223.

Stefanidou, M., Konopisi, S., Katakalos, K., Melidis, L., Koukouviki, A.M., 2026. Laboratory Investigation for Compatible Restoration of the Antiquities at the Venizelos Metro Station in Thessaloniki After their Removal, vol. 66. RILEM Bookseries, pp. 385–396. https://doi.org/10.1007/978-3-032-14170-5_38/FIGURES/11.

SUBLime, 2021. Sustainable Building Lime Applications via Circular Economy and Biomimetic Approaches. Welcome to SUBLime, a Marie Skłodowska-Curie Action European Training Network – Innovative Training Network (ETN ITN).

Swenson, E.G., Sereda, P.J., 1968. Mechanism of the carbonatation shrinkage of lime and hydrated cement. J. Appl. Chem. 18, 111–117. https://doi.org/10.1002/JCTB.5010180404.

Van Balen, K., 2005. Carbonation reaction of lime, kinetics at ambient temperature. Cement Concr. Res. 35, 647–657. https://doi.org/10.1016/J.CEMCONRES.2004.06.020.

Veiga, R., 2017. Air lime mortars: what else do we need to know to apply them in conservation and rehabilitation interventions? A review. Constr. Build. Mater. 157, 132–140. https://doi.org/10.1016/J.CONBUILDMAT.2017.09.080.

Veiga, R., Faria, P., van Hees, R., Stefanidou, M., Maravelaki, P.N., Ioannou, I., Theodoridou, M., Bokan Bosilijkov, V., Bicer-Simsir, B., et al., 2023. Rilem TC 277-LHS: specifications for testing and evaluation of lime-based repair materials for historic structures. Mater. Struct. 56.

von Greve-Dierfeld, S., Lothenbach, B., Vollpracht, A., Wu, B., Huet, B., Andrade, C., Medina, C., Thiel, C., Gruyaert, E., Vanoutrive, H., Saéz del Bosque, I.F., Ignjatovic, I., Elsen, J., Provis, J.L., Scrivener, K., Thienel, K.-C., Sideris, K., Zajac, M., Alderete, N., Cizer, Ö., Van den Heede, P., Hooton, R.D., Kamali-Bernard, S., Bernal, S.A., Zhao, Z., Shi, Z., De Belie, N., 2020. Understanding the carbonation of concrete with supplementary cementitious materials: a critical review by RILEM TC 281-CCC. Mater. Struct. 53 (6), 1–34. https://doi.org/10.1617/S11527-020-01558-W.

Wilkinson, M.D., Dumontier, M., Aalbersberg, IjJ., Appleton, G., Axton, M., Baak, A., Blomberg, N., Boiten, J.W., da Silva Santos, L.B., Bourne, P.E., Bouwman, J., Brookes, A.J., Clark, T., Crosas, M., Dillo, I., Dumon, O., Edmunds, S., Evelo, C.T., Finkers, R., Gonzalez-Beltran, A., Gray, A.J.G., Groth, P., Goble, C., Grethe, J.S., Heringa, J., t Hoen, P.A.C., Hooft, R., Kuhn, T., Kok, R., Kok, J., Lusher, S.J., Martone, M.E., Mons, A., Packer, A.L., Persson, B., Rocca-Serra, P., Roos, M., van Schaik, R., Sansone, S.A., Schultes, E., Sengstag, T., Slater, T., Strawn, G., Swertz, M. A., Thompson, M., Van Der Lei, J., Van Mulligen, E., Velterop, J., Waagmeester, A., Wittenburg, P., Wolstencroft, K., Zhao, J., Mons, B., 2016. Comment: the FAIR guiding Principles for scientific data management and stewardship. Sci. Data 3, 1–9.

Zhang, Y., Hubler, M., 2020. Role of early drying cracks in the shrinkage size effect of cement paste. J. Eng. Mech. 146, 04020128. https://doi.org/10.1061/(ASCE)EM.1943-7889.0001861.